Tailoring Widely Used Ammonia Synthesis Catalysts for H and N Poisoning Resistance

Journal:	*Physical Chemistry Chemical Physics*
Manuscript ID	CP-ART-09-2018-005800.R2
Article Type:	Paper
Date Submitted by the Author:	25-Jan-2019
Complete List of Authors:	Ghuman, Kulbir; Kyushu University, International Institute for Carbon-Neutral Energy Research Tozaki, Kota; Kyushu University, Department of Chemistry, Graduate School of Science Sadakiyo, Masaaki; Kyushu University, International Institute for Carbon-Neutral Energy Research (WPI-I2CNER) Kitano, Sho; Kyushu University, International Institute for Carbon-Neutral Energy Research Oyabe, Takashi; Kyushu University, Department of Chemistry, Graduate School of Science Yamauchi, Miho; Kyushu University, International Institute for Carbon-Neutral Energy Research

Journal Name

ARTICLE

Tailoring Widely Used Ammonia Synthesis Catalysts for H and N Poisoning Resistance

Received 00th January 20xx,
Accepted 00th January 20xx

DOI: 10.1039/x0xx00000x

www.rsc.org/

Kulbir Kaur Ghuman,[a]* Kota Tozaki,[b] Masaaki Sadakiyo,[ab] Sho Kitano,[a] Takashi Oyabe,[b] and Miho Yamauchi[ab]*

Despite many advancements, an inexpensive ammonia synthesis catalyst free from hydro-gen and nitrogen poisoning, and capable of synthesizing ammonia under mild conditions is still unknown and is long sought-after. Here we present an active nanoalloy catalyst, RuFe, formed by alloying highly active Ru and inexpensive Fe, capable of activating both N_2 and H_2 without blocking the surface active sites thereby overcoming the major hurdle faced by the current best performing pure metal catalysts. This novel RuFe nanoalloy catalyst operates under milder conditions than the conventional Fe catalyst and is less expensive than the so far best performing Ru-based catalysts providing additional advantages. Most importantly, by integrating theory and experiments, we identified the underlying mechanisms respon-sible for lower surface poisoning of this catalyst, which will provide directions for fabricat-ing poison-free efficient NH_3 synthesis catalysts in future.

Introduction

Ammonia (NH_3) is a strategic chemical produced in large quantities, most of which is used as a fertilizer to support food production. Currently, NH_3 is synthesized through Haber-Bosh process operated at 400-600 °C and 20-40 MPa and uses Fe catalyst, along with H_2 produced from steam reforming of hydrocarbons. This process contributes around one-third to the overall greenhouse gas emissions[1], challenging many researchers to work towards finding an alternative, sustainable and efficient NH_3 synthesis catalyst. Among many catalysts, Ru-based catalysts have attracted a lot of attention as they can synthesis NH_3 efficiently under milder conditions as compared to the conventional Fe catalyst used in Haber-Bosch process currently[2-5]. However, despite the excellent catalytic activity, Ru based catalysts get easily deactivated due to H-poisoning of the catalyst surface, suppressing the industrialization of Ru catalysts for mass production of NH_3. Some very recent Ru-based catalysts include Ru/C12A7e$^-$, where C12A7e$^-$ works as an excellent electron donor and reversible hydrogen-storage material,[6] and Ru/Pr_2O_3 which contain low-crystalline Ru nano-layers formed by reaction between Ru and strong basicity of Pr_2O_3.[7] In these catalysts the synergistic interaction between Ru and its support reduces the deterioration of the catalyst due to H-poisoning as well as accelerates the cleavage of the N≡N bond of N_2 thereby reducing the barrier for the rate-determining step of NH_3 synthesis reaction.

For the enhancement of durability of ammonia synthesis catalysts, in this work we choose a simple strategy where we alloyed high performance Ru catalyst that interacts weakly with N, with inexpensive Fe catalyst that interacts strongly with N, to design a rational NH_3 synthesis catalyst with distinct properties.[3] This strategy is simple yet very difficult to execute due to the large difference in the oxidation-reduction potentials of Ru and Fe ions, i.e., 0.455 V for Ru/Ru^{2+} and -0.447 V for Fe/Fe^{2+}, making it impossible until now to chemically reduce Ru and Fe to solid solution type Ru-Fe alloys containing more than 50atom% Fe. In this work, we demonstrate the synthesis of a well-mixed Ru-Fe nanoalloy supported on MgO (Ru-Fe/MgO) by using modified thermal decomposition method. The newly synthesized Ru-Fe/MgO catalyst with 50% composition from each Ru and Fe (denoted as RuFe), exhibits higher NH_3 production efficiency and lower poisoning than both pure Ru and Fe catalysts as long as we compare catalytic performances without promoters and focus only on intrinsic activities of the catalyst. The underlying mechanisms explaining the origin of higher performance and lower poisoning of RuFe nanoalloy catalyst is discussed in the following paper.

Results and discussion

We prepared the Ru-Fe/MgO catalysts by hydrogen reduction of precipitates produced on MgO supports via thermal decomposition of impregnated carbonyl complexes of Ru and Fe ions (details in Supplementary Information (SI)). In this method, metal compositions were controllable by changing a mixing ratio of metal complexes (Table S1). Both MgO supported Ru and Fe nanoparticles catalysts (Ru/MgO and Fe/MgO, respectively) were prepared in a similar way. X-ray diffraction measurements suggested that metallic phases are formed on all prepared catalysts (Fig. S1).

Scanning electron microscope (STEM) images for Ru/MgO, RuFe/MgO, and Fe/MgO are shown in **Fig. 1a**, **1b** and **1c**, respectively (see also **Fig. S2**). On these three catalysts, we can see nanoparticles well dispersed on MgO supports. Average diameter of the Ru, RuFe

[a] *International Institute for Carbon-Neutral Energy Research (WPI-I2CNER), Kyushu University, Motooka 744, Nishi-ku, Fukuoka 819-0395, Japan.*
E-mail: kulbirghuman@i2cner.kyushu-u.ac.jp
[b] *Department of Chemistry, Graduate School of Science, Kyushu University, Motooka 744, Nishi-ku, Fukuoka 819-0395, Japan*
E-mail: yamauchi@i2cner.kyushu-u.ac.jp
Electronic Supplementary Information (ESI) available:. See DOI: 10.1039/x0xx00000x

and Fe particles on MgO were calculated to be 6.2±2.1, 19±5.7, and 58±9.2 nm, respectively, i.e., nanoparticles formed on Ru-Fe/MgO catalysts have diameter between those of Ru and Fe nanoparticles (**Table S2**). We performed energy dispersive X-ray (EDX) measurements to clarify distribution of Ru and Fe atoms in the nanoparticle (**Figs. 1d**, **1e**, **1f** and **S3**). In **Figs. 1d** and **1e**, Ru and Fe ions, which are shown in red and green respectively, seem to be uniformly distributed, resulting in mostly yellowish nanoparticles originated from the overlap of red-colored Ru and green-colored Fe (**Fig. 1f**). X-ray photoelectron spectroscopy measurements for catalysts reduced under flowing H_2 clarified that the surface on RuFe/MgO includes metallic Ru and Fe species while surface of Fe/MgO is completely oxidized (**Fig. S4**), implying that Ru promotes reduction of Fe species.

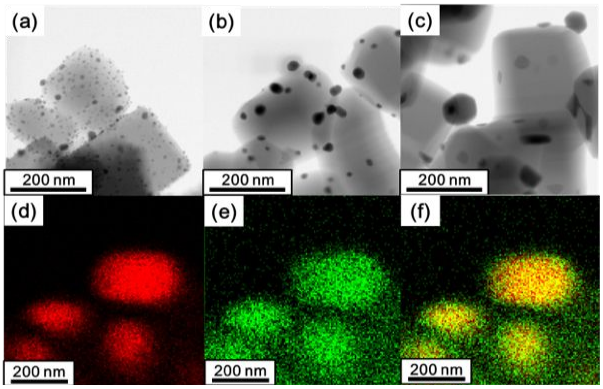

Fig. 1. STEM images for (a) Ru/MgO, (b) RuFe/MgO and (c) Fe/MgO and (d-f) EDX maps for RuFe/MgO. (d) Distributions of Ru (red) and (e) Fe (green) and (f) overlay of (d) and (e).

Next, we synthesized NH_3 using prepared catalysts in the temperature range from 300 to 600 ˚C under 0.1, 0.5 and 1 MPa. Catalytic performances at 400 ˚C for Ru-Fe/MgO with various compositions of Ru and Fe are represented in **Fig. S5**. Surprisingly, among all the prepared catalysts, RuFe/MgO exhibited the highest catalytic performance under 0.5 and 1 MPa whereas we could not observe any products on Fe/MgO, suggesting that Fe/MgO cannot promote NH_3 synthesis reaction under the conditions applied here. Temperature dependences of the turn over frequency (TOF) for NH_3 synthesis on Ru/MgO and RuFe/MgO are provided in **Fig. 2**. As mentioned above, particle sizes of the three catalysts are considerably different and simultaneous evaluation for active surface areas of Ru and Fe on alloy catalysts has not been achievable at present stage due to their different adsorption conditions and adsorption energy for CO or H_2.[8, 9] Thus, we normalized catalytic performance using surface area of catalysts, which were calculated from average diameters of the particles in STEM images. Under 0.1 MPa, TOFs on Ru/MgO and RuFe/MgO below 400 C seemed almost the same, i.e., 3.0×10^{16} and 4.1×10^{16} NH_3 molecule m^{-2} s^{-1}, respectively. Meanwhile, at 500 ºC, RuFe/MgO showed twice the performance on Ru/MgO, i.e., TOFs on Ru/MgO and RuFe/MgO were 8.1×10^{16} and 1.9×10^{17} NH_3 molecule m^{-2} s^{-1}, respectively. Furthermore, under 1 MPa at 600 ˚C, RuFe/MgO showed three times higher performance compared to that on Ru/MgO, suggesting that the alloying effect on the performance was pronounced at higher pressures and temperatures where influence from the surface poisoning becomes conspicuous. We further conducted catalytic reactions by changing partial pressure of reaction gas, N_2 and H_2, or product gas, NH_3, and calculated a reaction order for each gas. We

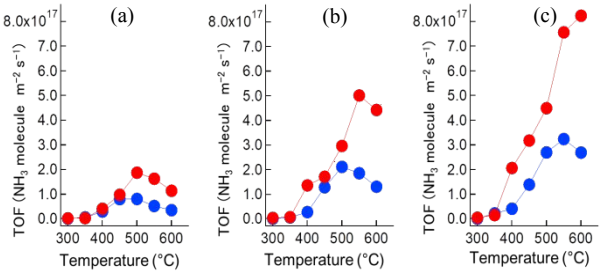

Fig. 2. Catalytic performance of Ru/MgO (blue) and RuFe/MgO (red) for NH_3 synthesis at (a) 0.1 MPa, (b) 0.5 MPa and (c) 1.0 MPa. Reaction conditions: catalyst 0.2g; reactant gas, H_2/N_2 =3 with a flow rate of 60 $mLmin^{-1}$; reaction temperature, 300~600 ˚C.

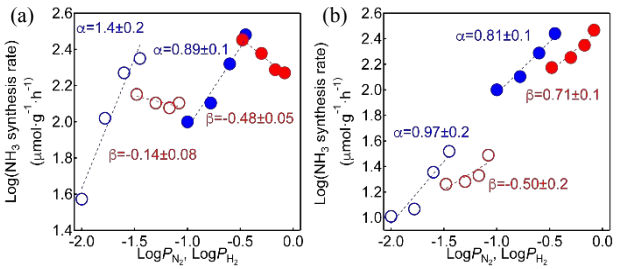

Fig. 3. Reaction orders of N_2 (α) and H_2 (β) on (a) Ru/MgO and (b) RuFe/MgO at 400 ˚C. Total pressure of reaction gases and total flow rate were 0.1 (open circle) or 1 MPa (filled circle) and 60 $mLmin^{-1}$.

applied an equation for NH_3 synthesis to a general formula of the reaction kinetics and found the reaction order α (or β) with N_2 (or H_2) on Ru/MgO and RuFe/MgO. **Figs. 3a** and **3b** represent that the amount of NH_3 produced while changing the partial pressure of N_2 or H_2 on Ru/MgO and Ru-Fe/MgO, respectively. Reaction orders for N_2 on Ru/MgO and RuFe/MgO below 0.1 (1.0) MPa of the reaction pressure were calculated to be 1.4 (0.89) and 0.97 (0.81), respectively, which implies that higher pressure of N_2 accelerates catalytic reactions both on Ru/MgO and RuFe/MgO. However, the corresponding reaction order on Ru/MgO for H_2 was -0.14 (-0.48), suggesting that Ru catalyst is relatively easily poisoned with H_2 gas under higher pressures. In contrast, the order on RuFe/MgO for H_2 is 0.50 (0.71), suggesting that the poisoning from H_2 is suppressed on RuFe/MgO and higher pressures of H_2 exhibit a positive influence on NH_3 synthesis, which contributes to increase in TOF on RuFe/MgO (**Fig. 2**).

To identify the origin of the low surface poisoning and high catalytic performance on RuFe alloy catalyst contrary to Ru and Fe metal catalysts, we conducted an in-depth theoretical calculation for NH_3 production reaction on both Ru and RuFe catalysts using density functional theory (DFT). Since RuFe alloy and Ru consist of an hcp structure,[10] we used Ru hcp structure to model the Ru and the alloy catalysts. For preparing Ru catalyst, we considered (0001) surface of Ru (**Fig. 4a**) as it is typically the lowest surface energy plane of Ru and hence the most abundant surface on most particles. For modelling alloy surface, we replaced 50% of Ru atoms with Fe atoms (**Fig. 4b**) as experimentally highest catalytic activity is obtained for the alloy having 50 at% of both Ru and Fe atoms (**Fig. S5**). The adsorbates are placed on the top layer of the slab at the various adsorption sites. Throughout this work, the plane-wave-pseudopotential approach was utilized,[11-17] details of which are given in SI.

Since the TOF for the NH_3 production depends on the binding energy of the reactants, intermediates and products to the active site, first we investigated the active sites for the N_2, N, H, H_2, NH, NH_2, and NH_3 by calculating the adsorption energies and preferred geometries on both Ru and RuFe catalyst surfaces. As shown in **Fig. 4a**, there are four adsorption sites on Ru: top of Ru (T), the bridge between two Ru atoms (B), the three-fold hcp hollow (H) and the threefold fcc hollow (F). The most stable adsorption sites for N_2, N, H, NH, NH_2, and NH_3 are T, H, F, H, B, and T, respectively. These most stable sites on Ru surface found in the calculations are in good agreement with the suggested sites in the literature.[18-23] The distance of N from Ru surface was found to be 1.05 ± 0.05 Å experimentally,[20] which also agrees well with our calculations (**Table S4**). As expected, both NH_3 and N_2 prefer to bind to the T site of Ru surface due to the electrostatic interaction between the electron-rich N atom having a lone pair and the most electron-deficient site on the surface. While in pure Ru only a few non-equivalent absorption sites can be found, the presence of Fe atoms in the RuFe alloy leads to several possible adsorption sites at: (1) top of Ru (T-Ru), (2) top of Fe (T-Fe), (3) Ru-Ru-Ru-Fe hcp (H-Ru3Fe), (4) Fe-Fe-Fe-Ru hcp (H-Fe3Ru), (5) Ru-Ru-Fe fcc (F-Ru2Fe), (6) Fe-Fe-Ru fcc (F-Fe2Ru), (7) Ru-Ru Bridge (B-RuRu), (8) Ru-Fe bridge (B-RuFe), and (9) Fe-Fe bridge (B-FeFe) (**Fig. 4b**). The most stable adsorption sites for N_2, N, H, NH, NH_2, and NH_3 adsorption on the RuFe alloy surface were found to be T-Ru, H-Fe3Ru, F-Ru2Fe, F-Fe2Ru, B-RuFe, and T-Ru, respectively. The adsorption energies and geometries for the most favorable adsorption sites for the intermediates of NH_3 synthesis reaction on Ru and RuFe surfaces are summarized in **Table S4** and **Table S5**, respectively. As alloying expands the lattice which in-turn reduces the deformation cost of the lattice due to the introduction of adsorbates, RuFe surface showed slightly higher binding energy with the adsorbates (except NH_3) compared to the Ru surface.

To analyze the surface activity of the alloy surface compared to the Ru surface, we conducted spin-density calculations (**Fig. S6**) which revealed that alloying leads to unpaired spin on the Fe atoms. Fe-induced spin polarization can be understood from the variation of the Fe-Ru bond length and the variation of the Fe atomic charge. The variation in bond length between atoms of alloy results in the

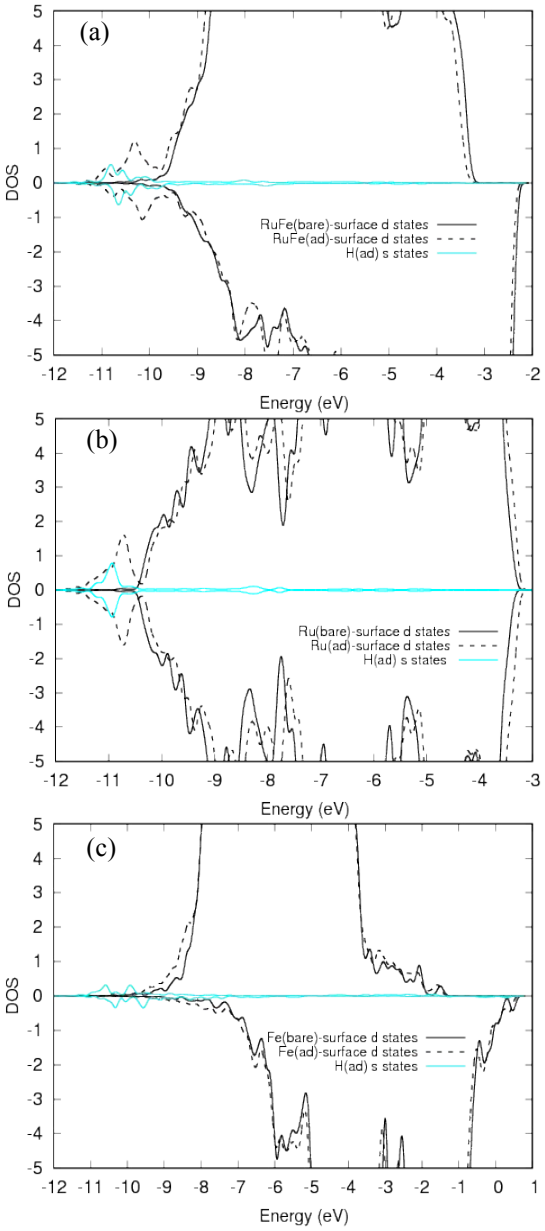

Fig. 5. The density of states of the adsorbed H species (cyan), and d-PDOS of the first layer atoms of (a) Ru, (b) RuFe, and (c) Fe surfaces before (black continuous) and after (black dotted) hydrogen adsorption. The positive and negative values represent spin-up and spin-down states, respectively.

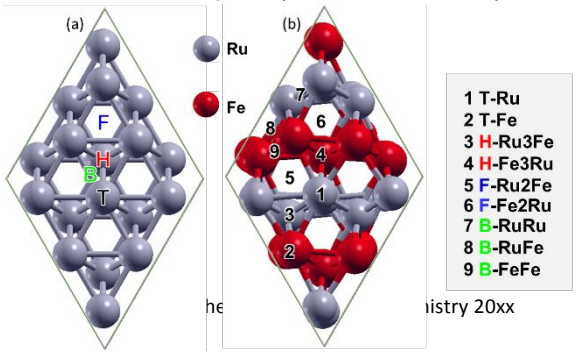

Fig. 4. Top view of supercell representing (a) Ru (0001) and (b) RuFe alloy surfaces along with the unique adsorption sites. Ru and Fe atoms are highlighted in grey, and red, respectively.

reduction in the covalent bond strength and enhancement in the ionic bonding interaction, thus giving rise to the unpaired electrons accumulation of unpaired electrons making the RuFe surface more active than Ru surface. This analysis is also in accordance with the results obtained from the Bader charge calculations,[24] which showed that approximately 0.3 electrons from Fe shift to Ru in the RuFe alloy. This is not an unexpected result as the electronegativity of Ru (2.3) is higher than that of Fe (1.83). We further confirmed the charge transfer direction by conducting work function calculations (**Fig. S7**) which showed that Fe surface has lower (3.45 eV) work function compared to Ru surface (4.57 eV) rationalizing the electron transfer from Fe to Ru when two metals are mixed together. In addition, RuFe surface showed work function (4.23 eV) higher than Fe surface and lower than Ru surface, as expected.

To further explain the comparatively higher activity of alloy surface we present in **Fig. S8** the partial density of states (PDOS) projected on the d-orbital of Ru, RuFe and Fe catalysts, along with their calculated spin up and spin down d-band centers (vertical line). Clearly, the d-band of RuFe shifted upwards compared to the d-band of Ru and shifted downwards compared to the d-band of the Fe. The five-fold degenerate d-states of the alloy catalyst (**Fig. S9**) revealed that the three-fold degenerate t_{2g} (d_{xz}, d_{yz}, d_{zx}) states are more responsible than the 2-fold degenerate e_g ($d_{x^2-y^2}$ and d_{z^2}) states for the narrower d-band near the d-band center. This appropriately tuned d-band of the alloy catalyst makes it highly active for NH_3 production and helps in reducing the hydrogen and nitrogen poisoning of alloy catalyst in contrast to Ru and Fe catalysts, respectively, which get poisoned easily with H and N species, respectively.

To analyze (H, N)-poisoning of the Ru, RuFe and Fe catalysts, we further analyzed the H-catalyst and N-catalyst interactions by calculating the d-PDOS of the surface atomic layer of Ru, RuFe and Fe catalysts with and without adsorbates (H, N). **Fig. 5** indicates that the d-band structure changes significantly upon H adsorption on all the three catalysts. However, this change in d-states due to overlap with H s states, which represents the strength of H-catalyst interaction, is maximum for Ru catalyst and is reduced for RuFe catalyst explaining the H-resistivity of RuFe catalyst compared to Ru catalyst, observed in experiments. Furthermore, on comparing the filled and the empty d states of the three catalysts with that of N p states, we found that only Fe is capable of donating electrons to the empty N orbitals due to its appropriate Fermi level (E_f) (**Fig. 6**), leading to strong Fe-N interaction and thus higher N-poisoning of Fe catalyst as compared to Ru and RuFe catalysts. Fermi level on RuFe is located at slightly lower energy but the nearest among three, implying that RuFe catalyst is capable to efficiently activate N_2 without severe N-poisoning.

We calculated the barrier for N adsorption on Ru, Fe, and RuFe surfaces to quantify the activity of RuFe surface as compared to Ru and Fe catalysts (**Fig. S10**). The energies are shown as a function of the relative number of Ru neighbors in the active site, denoted by z. The most stable adsorption site for N is the top of Ru for both Ru and RuFe surfaces. For Fe surface, we chose the geometry for N/Fe shown in **Fig. S11**, as this geometry was reported to be the most stable one for N adsorption on Fe catalyst.[25] For RuFe surface z corresponds to a value of (Ru/(Ru + Fe)) 0.71 as it has 5 Ru and 2 Fe neighbors in the first and the second atomic layers. For Ru and Fe surfaces, z is 1 and 0, respectively. Clearly, as expected,[3] the interaction energy between N adsorbate and RuFe surface is intermediate between that of the constituents and a distribution of bond energies will exist for a given distribution of sites on RuFe catalyst.

There are several indications in the literature that electrochemical catalysts, molecular catalysts as well as naturally occurring nitrogenase enzymes reduce N_2 via associative adsorption (or hydrogenation of N_2), rather than the dissociative adsorption (where N_2 molecules are first dissociated followed by subsequent addition of hydrogen).[26-30] Therefore, next we investigated the overall reaction energetics for NH_3 synthesis on both Ru and RuFe surfaces by analyzing the associative mechanism in which only H_2 molecules dissociate and NH_3 is formed by adding hydrogen atoms to the N_2 molecule (**Fig. 7**) for both surfaces. First NH_3 molecule is formed after the addition of five H atoms, followed by the formation of the second NH_3 molecule after adding the sixth hydrogen. **Fig. 7** shows that the stable N_2H_2 and N_2H_4 intermediates on Ru surface become unstable on RuFe surface along with unstable N_2H, and N_2H_3 intermediates and the overall reaction is exothermic on both surfaces. Further, formation of N_2H seems to be the rate-limiting step on Ru (as also reported in Ref. 26) and RuFe surfaces. However, on RuFe surface the barrier to form N_2H reduces by 1.98 eV compared to that on Ru surface justifying the better catalytic activity observed experimentally on RuFe alloy catalyst. We found similar results for the catalytic activity of Ru and RuFe surfaces for NH_3 synthesis even if the reaction proceeds via dissociative mechanism (refer SI, **Fig. S12**). In addition, the rate-limiting step (i.e. N_2 dissociation) for

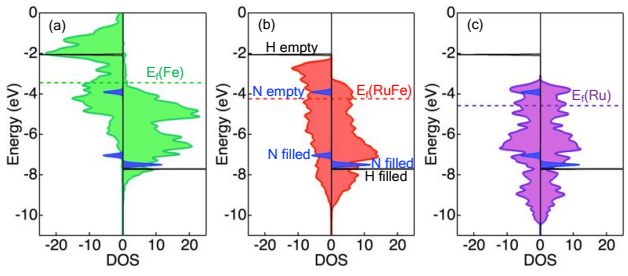

Fig. 6. The d-band PDOS of the first atomic layer of the (a) Fe, (b)RuFe, and (c)Ru surfaces along with their Fermi Energies (E_f, broken line) is represented . The p states of adsorbed N and s states of adsorbed H are represented in blue and black, respectively. The positive and negative values represent spin-up and spin-down states, respectively. The energy bands of Fe, RuFe, Ru, N and H are referenced to same vacuum level.

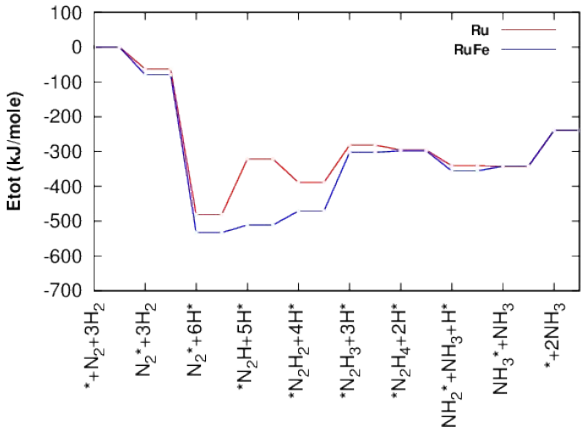

Fig. 7. Diagram showing energies of the intermediates of the NH_3 synthesis reaction on Ru and RuFe surfaces via associative mechanism. "*" stands for an empty site on the surface.

dissociative mechanism showed lower energy barrier on RuFe surface compared to the Ru surface (**Fig. S13**).

Conclusions

We demonstrated a novel (H, N)-poisoning resistant RuFe alloy catalyst having higher catalytic efficiency for ammonia synthesis than traditional metal (Ru and Fe) catalysts. Alloying seems to exert significant impacts under higher pressures where reasonable conversion rates for NH_3 production are practically achievable. Since we could not observe any conversion on Fe/MgO at the temperatures and pressures at which Ru/MgO is usually activated, RuFe/MgO exhibited higher activity at temperatures higher than at which Ru/MgO catalyst is active. The role that mixing of two metals played in the thermochemical activation of N_2 and H_2 to form NH_3 was investigated through comprehensive DFT study, which showed that the lattice deformation and the unique d-band structure originated from alloying Ru with Fe is responsible for better activity and (N, H)-poisoning resistance of the RuFe catalyst. Although the performance of simple RuFe/MgO catalyst is not higher to make it commercially attractive (**Table S3**), further modulation of the catalyst will enhance its activity to meet requirements for practical applications, e.g., introduction of appropriate promoters or supports.[31] Furthermore, this detailed experimental and theoretical study not only provides a novel catalyst for ammonia synthesis but also provides new insights that will inspire the development of next-generation, durable and efficient, ammonia synthesis catalysts.

Conflicts of interest

There are no conflicts to declare.

Acknowledgements

This work was supported by the International Institute for Carbon Neutral Energy Re-search (WPI-I^{2}CNER), sponsored by the World Premier International Research Center Initiative (WPI). This work was supported by MEXT KAKENHI Grant Number JP12852953 and JP18H05517, JST-CREST, and MEXT, Japan. The computations were performed by using Computational Science Research Center, Okazaki, Japan and the HPC supercomputer at International Institute for Carbon Neutral Energy Research (I2CNER), Kyushu University, Japan. The authors thank Prof. K. Nagaoka (Oita University)and Prof. K. Sato (Kyoto University) for their useful advices regarding ammonia synthesis experiments.

Notes and references

1 M. Appl, Ullmann's Encyclopedia of Industrial Chemistry, Ammonia, Wiley-VCH Verlag GmbH & Co. KGaA, Weinheim, 2006.
2 K. Aika, A. Ozaki, H. Hori, J. Catal. 1972, **27**, 424.
3 C.J.H. Jacobsen, S. Dahl, B.S. Clausen, S. Bahn, A. Logadottir, J.K. Nørskov, J. Am. Chem. Soc. 2001, **123**, 8404.
4 K. Aika, Catal. Today, 2017, **286**, 14.
5 Y. Kobayashi, Y. Tang, T. Kageyama, H. Yamashita, N. Masuda, S. Hosokawa, H. Kageyama, J. Am. Chem. Soc. 2017, **139**, 18240.
6 M. Kitano, Y. Inoue, Y. Yamazaki, F. Hayashi, S. Kanbara, S. Matsuishi, T. Yokoyama S. Kim, M. Hara, H. Hosono, Nat. Chem., 2012, **4**, 934.
7 K. Sato, K. Imamura, Y. Kawano, S. Miyahara, T. Yamamoto, S. Matsumura, Chem. Sci., 2017, **8**, 674.
8 O. Kubaschewski, O. In Iron-Binary phase diagrams, Springer-Verlag Berlin Heidelberg GmbH, 1982; pp 123.
9 Y.V. Larichev, B.L. Moroz, V.I. Zaikovskii, S.M. Yunusov, J. Phys. Chem. C 2007, **111**, 9427.
10 H-J. Jung, M.A. Vannice, L.N. Mulay, R.M. Stanfield, W. N. Delgass, J. Catal. 1982, **76**, 208.
11 J. Perdew, K. Burke, M. Ernzerhof, Phys. Rev. Lett. 1996, **77**, 3865.
12 D. Vanderbilt, Phys. Rev. B 1990, **41**, 7892.
13 P. Giannozzi, S. Baroni, N. Bonini, M. Calandra, J. Phys.: Condens. Matter 2009, **21**, 395502.
14 H. J. Monkhorst, J. D. Pack, Phys. Rev. B 1976, **13**, 5188.
15 G. Mills, H. Jonsson, G. K. Schenter, Surf. Sci. 1995, **324**, 305.
16 H. Jonsson, G. Mills, K. W. Jacobsen, Classical and Quantum Dynamics in Condensed Phase Simulations edited by B. J. Berne, G. Ciccotti, and D. F. Coker. World Scientific 1998, Singapore.
17 G. Henkelman, H.G. Jonsson, J. Chem. Phys. 2000, **113**, 9978.
18 K. Jacobi, H. Dietrich, G. Ertl, Appl. Surf. Sci. 1997, **121**,558.
19 M. Staufer, K. M. Neyman, P Jakob, V. A. Nasluzov, D. Menzel, N. RÃűsch, Surf. Sci. 1996, **369**, 300.
20 S. Schwegmann, A. Seitsonen, H. Dietrich, H. Bludau, H. Over, K. Jacobi, G. Ertl, Chem. Phys. Lett. 1997, **264**, 680.
21 H. Shi, K. Jacobi, Surf. Sci. 1994, **313**, 289.
22 M. Lindroos, H. Pfnür, P. Feulner, D.A. Menzel, Surf. Sci. 1987, **180**, 237.
23 Á Logadóttir, J.K. Nørskov, J. Catal. 2003, **220**, 273.
24 W. Tang, E. Sanville, G.A. Henkelmen, J. Phys.: Condens. Matter 2009, **21**, 084204.
25 J. Mortensen, M. Ganduglia-Pirovano, L. Hansen, B. Hammer, P. Stoltze, J.K. Nørskov, Surf. Sci. 1999, **422**, 8.
26 E. Skúlason E., T. Bligaard, S. Gudmundsdóttir, F. Studt, J. Rossmeisl, F. Abild-Pedersen, T. Vegge, H. Jónssonac, J.K. Nørskov, Phys. Chem. Chem. Phys. 2012, **14**, 1235.
27 G. Ertl, In Catalytic Ammonia Synthesis: Fundamentals and Practice, J. R. Jennings, Plenum Press, New York, 1991.
28 P. Stoltze, J.K. Nørskov, Phys. Rev. Lett. 1985, **55**, 2502.
29 A.L. Garden, E. Skúlason, J. Phys. Chem. C. 2015, **119**, 26554.
30 J.-C. Liu, X.-L. Ma, Y. Li, Y.-G. Wang, H. Xiao, J. Li, Nat. Comm. 2018, **9**, 1610.
31 P. Wang, F. Chang, W. Gao, J. Guo, G. Wu, T. He, P. Chen, Nat. Chem., 2017, **9**, 69.

Graphical Abstract

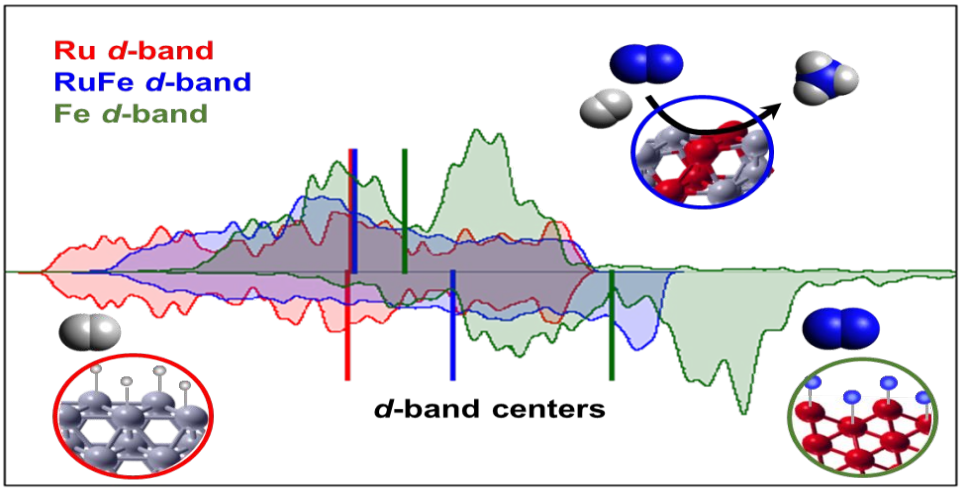

A novel (N, H)-poisoning resistant RuFe nanoalloy catalyst with a unique d-band structure originated from alloying Ru with Fe, providing a route to design new catalysts for ammonia synthesis.